Structural organization of ionic liquids embedded in fluorinated polymers

Viktor I. Petrenko[1,2], Liliana C. Fernandes[3], Oleksandr I. Ivankov[4,], Carmen R. Tubio[1], Mohammad Tariq[5], José M.S.S. Esperança[5], Daniela M. Correia[3]* and Senentxu Lanceros-Mendez[1,2,*]

[1]BCMaterials, Basque Center for Materials, Applications and Nanostructures, UPV/EHU Science Park, 48940 Leioa, Spain

[2]Ikerbasque, Basque Foundation for Science, 48009 Bilbao, Spain

[3]Centre of Physics Universities of Minho and Porto, University of Minho, 4710-058 Braga, Portugal

[4] Taras Shevchenko National University of Kyiv, 01601 Kyiv, Ukraine

[5]LAQV, REQUIMTE, Departamento de Química, Faculdade de Ciências e Tecnologia, Universidade Nova de Lisboa, 2829-516 Caparica, Portugal

[6]Centre of Chemistry, University of Trás-os-Montes e Alto Douro, 5001-801, Vila Real, Portugal

*Corresponding authors

D.M. Correia (d.correia@fisica.uminho.pt)

S. Lanceros-Méndez (senentxu.lanceros@bcmaterials.net)

Abstract

Hybrid materials based on ionic liquids (ILs) and polymers are increasingly being used for the development of smart and multifunctional materials, allowing to tune polymer properties or introduce new ones. Nonetheless, the structural organization of ILs within the polymer matrix is not properly understood. This work reports on the structural organization of different ILs incorporated into polyvinylidene fluoride (PVDF) films. The effect of IL type ([Pmim][TFSI], [Pmpip][TFSI], $[Bmim]_2[NiCl_4]$ and $[Bmim][FeCl_4]$) incorporated into the PVDF matrix on the structural organization was evaluated and correlated to the observed variations in the morphological and physical-chemical properties. $[Bmim][FeCl_4]$ and $[Bmim]_2[NiCl_4]$ leads to highly porous structures and the incorporation of ILs into the polymer matrix increases the electroactive β phase content of PVDF. Different structural organization of the hybrid materials at nanoscale has been found by small-angle neutron scattering experiments. Whereas just single polydisperse objects with average size of about 5 nm have been found in PVDF/[Pmim][TFSI] and PVDF/[Pmpip][TFSI] samples, more complex fractal-like organization of pores are present in PVDF/$[Bmim][FeCl_4]$ and PVDF/$[Bmim]_2[NiCl_4]$. Thus, IL type influences both the morphology and the electroactive phase of the polymer. Complex fractal-like organization observed for $[Bmim][FeCl_4]$ and $[Bmim]_2[NiCl_4]$ into the PVDF matrix allows a porous morphology, while single polydispersed particles of [Pmpip][TFSI] or [Pmpip][TFSI] into PVDF favors strong ion-dipole interactions between the IL and the polymer matrix, resulting in higher electroactive β phase contents.

Keywords: Ionic liquids, hybrid materials, PVDF, structural organization

1. Introduction

Smart materials provide a controllable, specific and reproducible variation of some physical-chemical properties upon an external stimulus [1] such as, stress, temperature, electric or magnetic field, among others. Due to their interesting ability to respond to the surrounding stimulus and their typically simple processing, including by additive manufacturing technologies, and integration into devices, polymer based smart materials have gained particular attention to be applied in different areas [2, 3].

To improve and/or add new functionalities to smart and multifunctional polymers, hybrid materials are developed by adding fillers such as nanoparticles, carbon nanotubes, proteins, or ionic liquids (ILs), among others, allowing the development of composites with tailored functional response [4].

In particular, ILs have been extensively studied for a wide range of applications, based on their large versatility and the possibility of precisely tailoring their physical-chemical characteristics [4]. ILs have been typically defined as salts entirely composed by anions and cations and with melting temperatures below 100 ºC. They are generally nonflammable, show negligible vapor pressure, high thermal, chemical and electrochemical stability, as well as high ionic conductivity [4, 5]. Additionally, due to the largest variety of cations and anions, it is possible to develop a wide range of functional ILs, allowing their applicability in a wide range of applications [6] including sensors and actuators [7-10], biomedicine [11, 12] and energy generation and storage [13, 14], among others.

Besides the high interest devoted to the development of IL-polymer based materials, there is a lack of studies concerning the materials characterization at nanoscale. Their characterization is mostly focused on the morphology, physico-chemical, electrical/ionic,

and mechanical characterization techniques [4, 15]. The study of the ILs structural organization into the polymer matrix will allow a better understanding of the IL-polymer matrix chain interactions, stability and macroscopic response. In this context, small-angle neutron (SANS) or X-ray (SAXS) scattering techniques are among the most suitable techniques. In fact, recently SANS and SAXS were successfully used for the detailed structural characterization at the nanoscale of native and modified (by magnetic nanoparticles) woven cotton textiles and different structural organization of nanoparticles were observed [16]. With respect to ILs, SANS studies have been reported, often relying on the study of the solvent and/or IL influence in the polymeric matrix structure/conformation, solvation and dispersion [17-19]. The combination of polyethylene glycol (PEG) and polyethylene oxide (PEO) with imidazolium-based ILs has been studied [19-25]. In particular, the solubility and conformability of PEG in cholinium amino acid-based (glycinate, prolinate and argininate) ([Ch][AA]) ILs and water mixtures was tested and it has been found that the hydrogen bond capacity of the anion plays a key role in the salting out effect of PEG and that the radius of gyration is dependent on the anions species and water concentration [20]. The solvation of PEO in different protic ionic liquids (PILs) was also studied by dissolving PEO in pure propylammonium nitrate (PAN) and PAN with a 10 % mole fraction of propylammonium chloride (PACl) or propylammonium bromide (PABr). A reduction in the solvation quality was observed by the addition of the halide salt in the order PAN>PABr>PACl, as well as an increase in the charge density (NO_3^- to Br^- to Cl^-), leading to a larger ionic interaction and, therefore, to a poorer solvation [19].

Attending to the previously mentioned and to the lack of studies concerning the IL-polymer interactions and structural organization at a nanoscale, this work reports on hybrid films based on polyvinylidene fluoride (PVDF) with different ILs types (different

anions and cations), in order to access the influence structural organization of the IL types within the polymer matrices and their effect in the properties of the composites. An IL content of 40% wt. has been incorporated in the polymer matrix, since higher concentrations lead to mechanically less stable samples and also limits incorporation of IL with the matrix. The morphological and physico-chemical properties of the developed materials were studied, together with SANS technique, in order to access the composite structure at a nano- and micro-scale.

2. Materials and methods

2.1.Materials

The 1-propyl-3-methylimidazolium bis(trifluoromethylsulfonyl) imide ([Pmim][TFSI]) (purity>90%), 1-methyl-1-propylpiperidinium bis(trifluoromethylsulfonyl) imide ([Pmpip][TFSI]) (purity>90%) and 1-butyl-3-methylimidazolium tetrachloroferrate ([Bmim][$FeCl_4$]) (purity>97%) were purchased from Iolitec. The bis(1-butyl-3-methylimidazolium) tetrachloronickelate ($[Bmim]_2[NiCl_4]$) was synthetized as described in [26, 27]. More specifically, 1-butyl-3-methylimidazolium chloride, [Bmim][Cl] (supplied by IOLITEC with a stated purity higher than 99%) was mixed in a 2:1 molar ratio with $NiCl_2 \times 6H_2O$ (acquired from Alfa Aesar with a purity level over 98%). Both compounds are solid at ambient temperature, so an ionic liquid aqueous solution was prepared before the addition of $NiCl_2$. After synthesis, water was removed in a rotavapor. The final drying procedure consists of vacuum-drying the sample for at least a day at moderate temperature (about 330 K) [26, 27]. PVDF 6010 (Mw=300 000−330 000 Da) was purchased from Solvay. N, N dimethylformamide (DMF) (99.5% purity) was purchased from Merck.

2.2.Sample preparation

The films were prepared by solvent casting following the general guidelines presented in [28]. For the preparation of the pristine polymer films, after completely PVDF dissolution in DMF (ratio of 15/85 % w/w polymer/solvent) under magnetic stirring at room temperature, the solution was spread into a glass, the solvent was evaporated at 210 ºC (P-Selecta model 2000208 oven) during 10 min and let to cool down to room temperature. After this procedure, PVDF crystallizes into the non-polar α-phase [28]. The polymer/IL composites were prepared after a similar procedure: prior to the polymer dissolution, 40 wt. % of the corresponding IL ([Pmim][TFSI]), [Pmpip][TFSI], $[Bmim]_2[NiCl_4]$ or [Bmim][$FeCl_4$]) was dispersed in DMF, under magnetic agitation, until a homogenous solution was obtained. Then, PVDF was added in a ratio of 15:85 wt. % (PVDF/DMF). After polymer dissolution, the solution was spread on a glass at room temperature, the solvent was evaporated at 210 °C for 10 min. For the composites PVDF/$[Bmim]_2[NiCl_4]$, and PVDF/[Bmim][$FeCl_4$], incorporating magnetic IL anions, mechanical agitation was used instead of magnetic agitation. After those procedures, films with 40% wt. of IL and an average thickness of ~33 μm were obtained.

2.3.Sample characterization

The morphology of the samples was evaluated by scanning electron microscopy (SEM) (Hitachi S-4800 field emission SEM, accelerating voltage of 10 kV). Previously, the films were coated with a thin gold layer by sputter coating (Polaron, model SC502).

The chemical characterization of the developed materials was performed by Fourier transform infrared spectroscopy (FTIR) technique in attenuated total reflection (ATR)

mode (JASCO FT/IR-6100) using 64 scans in the range from 600 to 4000 cm^{-1} and a resolution of 4 cm^{-1}. From the FTIR-ATR spectra the β phase content of the samples was evaluated using **equation 1**:

$$F(\beta) = \frac{A_\beta}{\left(K_\beta / K_\alpha\right) A_\alpha + A_\beta} \quad (1)$$

Where A_α and A_β are the absorbances at 766 and 840 cm^{-1}, respectively, and Kα and Kβ are the corresponding absorption coefficients (6.1×10^4 and 7.7×10^4 $cm^2\,mol^{-1}$).

Differential scanning calorimetry (DSC) was used to study the thermal properties of the samples (Mettler Toledo DSC 821e apparatus). The experiments were conducted between 20 and 300 ºC at a heating rate of 10 ºC·min^{-1} under nitrogen purge.

The thermal degradation of the composite films was studied by thermogravimetric analysis (TGA) (PerkinElmer TGA 4000) in the temperature range between 30 and 800 ºC at a heating rate of 10 ºC·min^{-1} in a nitrogen atmosphere.

SANS experiments were performed in the small-angle spectrometer YuMO at the IBR-2 pulsed reactor (JINR, Dubna, Russia) in the time-of-flight mode [29]. The differential cross section per sample volume (scattering intensity) was obtained as a function of the scattering vector module, $q=(4\pi/\lambda)\sin(\theta/2)$, where λ is the incident neutron wavelength and θ is the scattering angle. SANS curves were obtained using a wavelength range of λ=0.05÷0.8 nm. The absolute calibration of the scattered intensity was carried out by using vanadium standard and raw data were averaged using the SAS program [30]. The analysis of the SANS data was performed using SasView software [SasView version 5.0, http://www.sasview.org/].

3. Results and Discussion

3.1.Morphology

The morphology of neat PVDF polymers and the corresponding IL based composites is presented in the representative SEM images shown in **Figure 1**.

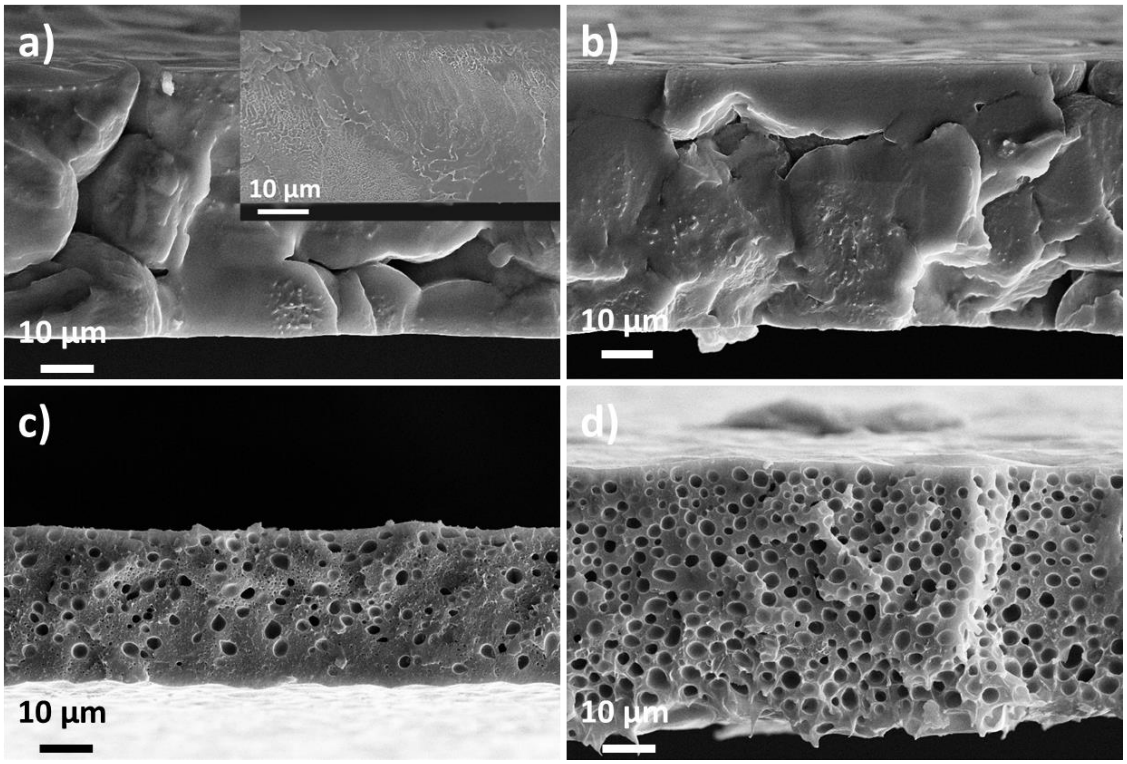

Figure 1 – Representative SEM cross-section images of the composite films comprising 40% wt. of the ILs: a) PVDF/[Pmim][TFSI] (inset: unmodified initial PVDF cross-section film), b) PVDF/[Pmpip][TFSI], c) PVDF/[Bmim][$FeCl_4$] and d) PVDF/$[Bmim]_2[NiCl_4]$.

The morphology of PVDF and hybrid composites strongly depend on the processing conditions, the obtained morphology being compatible with the used processing conditions of solvent evaporation at 210 ºC prior to polymer crystallization [31]. PVDF is obtained in the form of compact dense films, as corresponding to the used processing conditions [32]. The films are characterized by a homogeneous and non-porous surface (see inset of **Figure 1a**) [28]. Upon the [Pmim][TFSI] and [Pmpip][TFSI] incorporation,

PVDF/[Pmim][TFSI] and PVDF/[Pmpip][TFSI] films present a spherulitic structure characteristic of neat PVDF polymer films [33, 34], as shown in **Figure 1a** and **Figure 1b**, the result being independent of the IL cation type. On the other hand, the incorporation of [Bmim][$FeCl_4$] and $[Bmim]_2[NiCl_4]$ promotes the development of a well-defined porous structure (**Figure 1c and 1d**), which is a characteristic of magnetic ILs incorporation into PVDF matrix [15]. This porous structure is a consequence of the solvent-IL interactions, leading to a phase separation process. Further, due to the high dipole moment of DMF and the interaction with the IL, once solvent evaporation takes place, the ILs remains encapsulated in the pores lefts by the migration of the phase-separated solvent+IL [9, 15, 32]. These results are an indicative that the interactions between the solvent and the [Bmim][$FeCl_4$] and $[Bmim]_2[NiCl_4]$ are stronger than the interactions that occurs with [Pmim][TFSI] and [Pmpip][TFSI].

3.2.Physical-chemical properties

The influence of the IL type into the vibrational spectra of the PVDF based films was evaluated by FTIR-ATR measurements (**Figure 2a**).

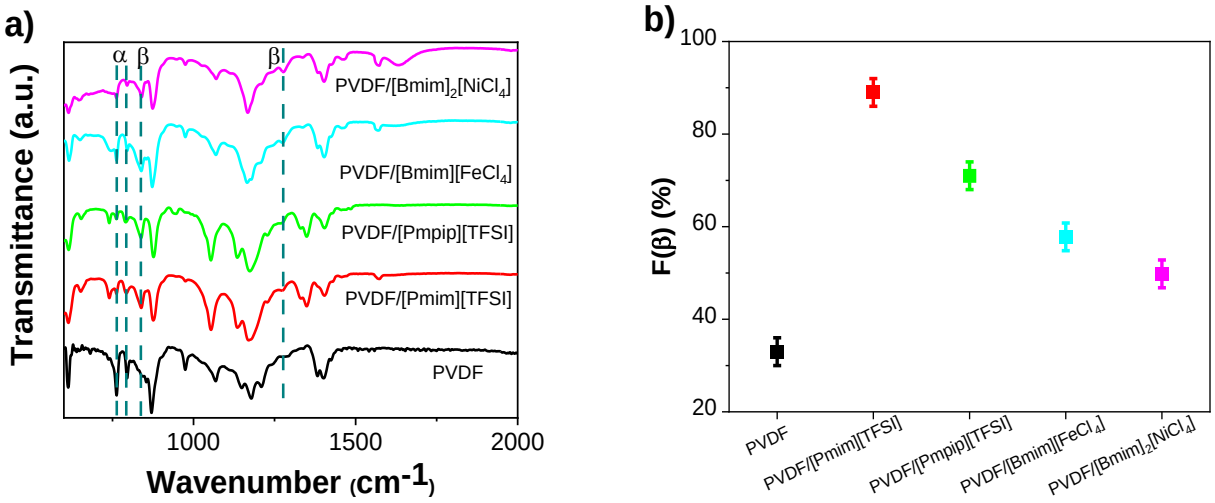

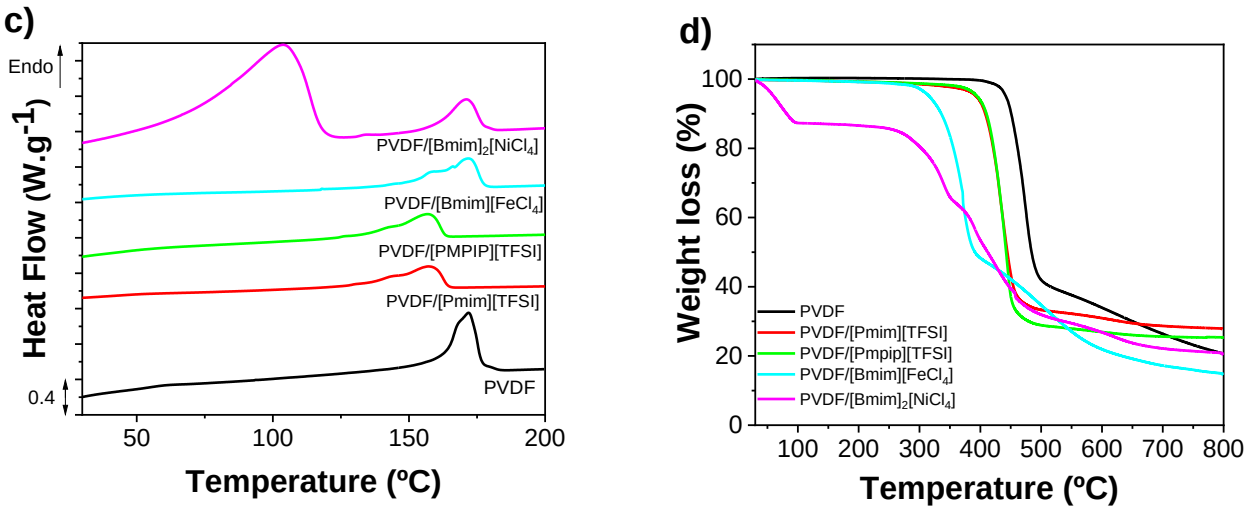

Figure 2. a) FTIR spectra, b) electroactive β phase content, c) DSC scans and d) TGA curves of the different PVDF/IL film composites: PVDF/[Pmim][TFSI], PVDF/[Pmpip][TFSI], PVDF/[Bmim][$FeCl_4$] and PVDF/[Bmim]$_2$[$NiCl_4$].

The FTIR-ATR spectra of the PVDF and PVDF based composites show the main characteristic PVDF absorption bands, namely the α phase bands at 795 and 976 cm^{-1}. Additionally, for all samples, the β-phase absorption band is observed at 840 cm^{-1} and 1275 cm^{-1} [35]. It is to notice that, after the selected processing conditions, neat PVDF crystallizes mainly in the α phase (67%) [28]. Upon ILs incorporation into PVDF matrix, and independently of the IL type, an increase in the intensity of the β phase characteristics absorption bands occur, described as an all-trans (TTT) planar zigzag conformation of PVDF chain, acting ILs as β phase nucleating agents due to the electrostatic interactions between the PVDF polymer chain with the positive and negative charges from the IL [9]. The β-phase content quantification of all the samples (**Figure 2b**) was evaluated using **equation 1**. As observed, independently of the IL type, the inclusion of an IL into the PVDF matrix induces the PVDF crystallization majorly in the electroactive β phase. The highest β phase content is observed for PVDF/[Pmim][TFSI] composite (89%), followed

by the composites PVDF/[Pmpip][TFSI] (71%), PVDF/[Bmim][$FeCl_4$] (58%) and PVDF/$[Bmim]_2[NiCl_4]$ (50%). The observed differences indicate that the interaction between the polymer chains and the IL charges is influenced by the IL type, namely the cation and anion, displaying the [Pmim][TFSI] strong interactions with PVDF polymer chain comparatively with the other ILs. Further, it is also to notice that for the composites comprising the ILs [Bmim][$FeCl_4$] and $[Bmim]_2[NiCl_4]$, the presence of two $[Bmim]^+$ cations in the IL $[Bmim]_2[NiCl_4]$ leads to slight decrease of the eletroactive phase as a result of the hinderance of interaction between the CF_2 groups of PVDF with the imidazolium $[Bmim]^+$ charges.

The presence of the IL within the polymer matrix is confirmed by the corresponding absorption bands: For the composites comprising the $[TFSI]^-$ anion, the absorption band present at 740 cm^{-1} is attributed to the cis $[TFSI]^-$ conformation, and at 1135 cm^{-1} and 1149 cm^{-1} due to the asymmetric and symmetric stretching vibration modes from the SO_2 group [36]. For the composites comprising the ILs sharing the same cation $[Bmim]^+$, the absorption band at 1168 cm^{-1} is attributed to the C-N vibration and the skeleton vibrations between 1327 cm^{-1} and 1600 cm^{-1} [37].

The DSC spectra of the composite films are presented in

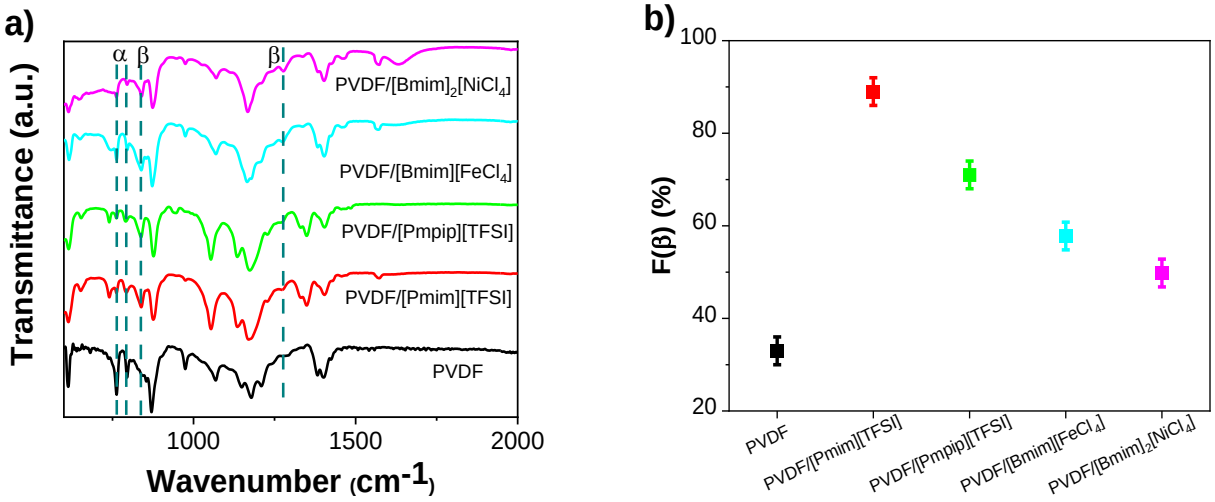

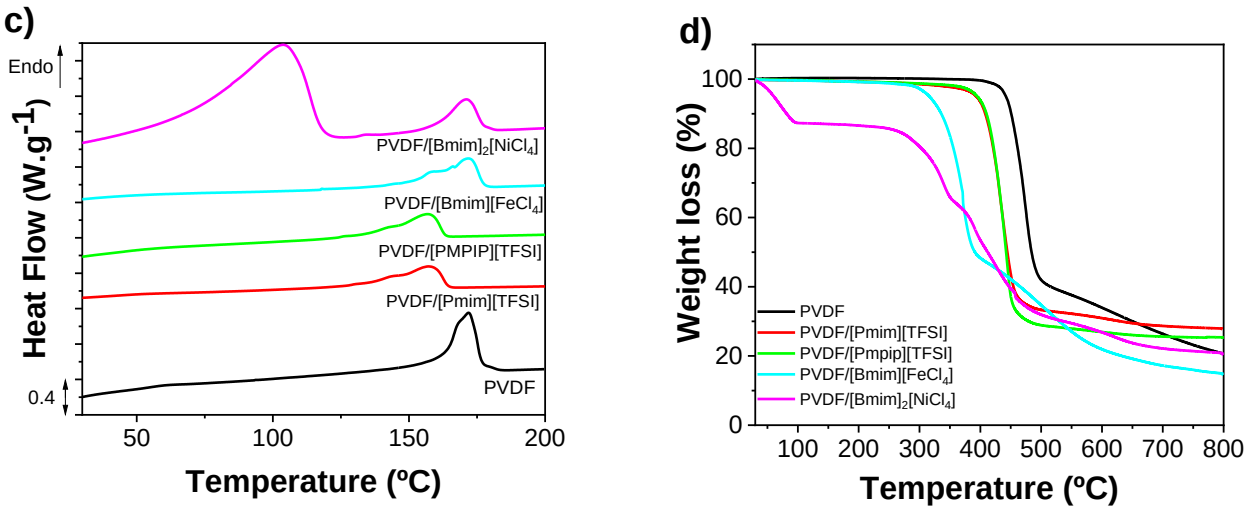

Figure 2c. Independently of the IL type, the composite films containing PVDF as the polymeric matrix present a single endothermic peak at ~157 ºC ascribed to the melting temperature of PVDF [34]. It is also to notice that, independently of the IL type, all the samples show a similar trend, with a single melting peak that shifts to lower temperatures, when compared with the melting temperature of the pristine PVDF polymer. The decrease in the melting temperature with the incorporation of the ILs indicated a destabilization of the crystalline phase of PVDF as a result of the electrostatic interactions between the different ILs and the PVDF chain, hindering the crystallization process [38].

The influence of the IL type and polymer matrix in the thermal degradation of the samples was evaluated by TGA measurements (

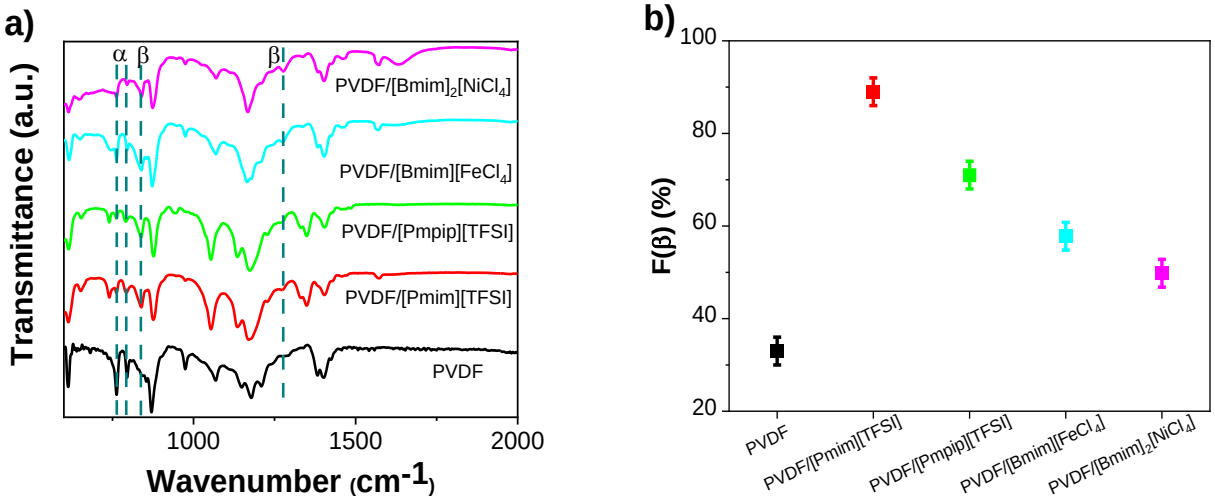

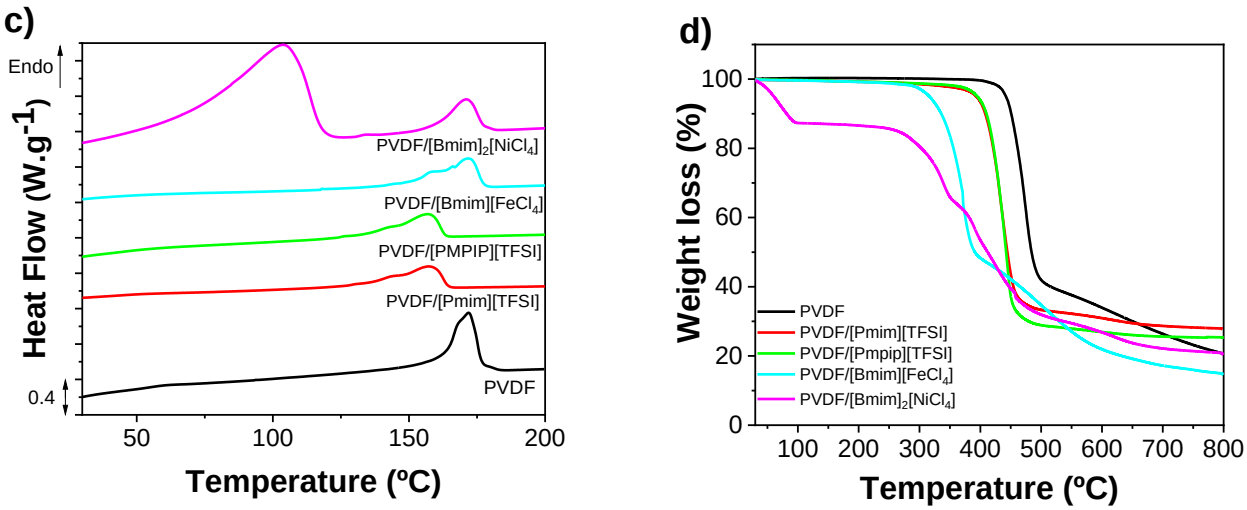

Figure 2d). The thermal degradation of PVDF occurs through C-H and C-F polymer chains decomposition in a single degradation step starting at ~ 450 ºC. Upon ILs incorporation into the PVDF matrix, it is observed that the PVDF composite films with [Pmim][TFSI] and [Pmpip][TFSI] display a single degradation step at ~ 400 ºC with a residual weight of 28 % and 25 %, respectively, associated to the thermal degradation of the polymer [34]. For PVDF/$[Bmim]_2[NiCl_4]$ the first weight loss, is attributed to water loss ascribed to the hydrophilic IL behavior [32]. The degradation step at ~330 ºC is attributed to the IL imidazolium cation through dealkylation degradation, finalizing with the PVDF polymer degradation. PVDF/$[Bmim][FeCl_4]$ samples display two degradation steps at ~330 ºC and 430 ºC associated to the $[Bmim]^+$ and PVDF thermal degradation, respectively [9]. In this context, independently of the IL type, a decrease in the thermal stability of PVDF matrix occurs upon the different ILs incorporation.

3.3.Structural organization of the IL within the polymer matrix

Small-angle neutron scattering measurements were conducted for the detailed structural characterization of the polymer-based composites with addition of various ILs as a filler. Experimental SANS curves for all PVDF/IL samples are presented in **Figure 3**, showing that all SANS data can be grouped in two categories. SANS from pure film is very low,

almost at the background level (data not shown), being not possible to conclude the nanoscale structure of neat PVDF film. The SANS data for PVDF/[Pmim][TFSI] and PVDF/[Pmpip][TFSI] show a scattering plateau at low q-values (reaching so-called Guinier regime [39]) and the PVDF/[Bmim][$FeCl_4$] and PVDF/$[Bmim]_2[NiCl_4]$ composites show a power-law decay at small q-values, reflecting the presence of large, extended structures with fractal-like organization [40, 41]. SANS curves are thus depending on the IL type, indicating the formation of various structures at the nanoscale. It should be noted that scattering objects for all samples are highly polydisperse, as smoothed curves are observed , which is typical for polydisperse systems, unlike the case of a highly symmetric system of monodisperse particles, which should give characteristic oscillations [39].

At sufficiently small q-values ($qRg < 1$), the scattered intensity can be described by the Guinier approximation [39]:

$$I(q) = I(0) \exp(-(qRg)^2/3) \quad (2)$$

with just two parameters, which are the forward scattered intensity, I(0) (which is proportional to the concentration; square of the contrast in scattering length density between matrix and inhomogeneity; and square of the particles volume), and the radius of gyration, Rg (characteristic size of the scattering objects).

The power-law decay of the SANS data was fitted by $I(q)=B \cdot q^{-p}$ and the value of the P exponent reflects the inner structure of the scattering units and characterizes the type of their mass or surface organization according to the following classification [42]:

$1 < P < 3$; mass fractal with fractal dimension, $Dm = P$.

$3 < P < 4$; surface fractal with fractal dimension, $Ds = 6 – P$.

4 < P < 6; diffusive surface with exponent, b = (P – 4) /2.

For mass fractal aggregates the following relation between aggregates volume, V, and its linear size, L, is obtained: $V \sim L^{Dm}$. And in the case of surface fractal, the surface, S, is proportional to the linear size as $S \sim L^{Ds}$.

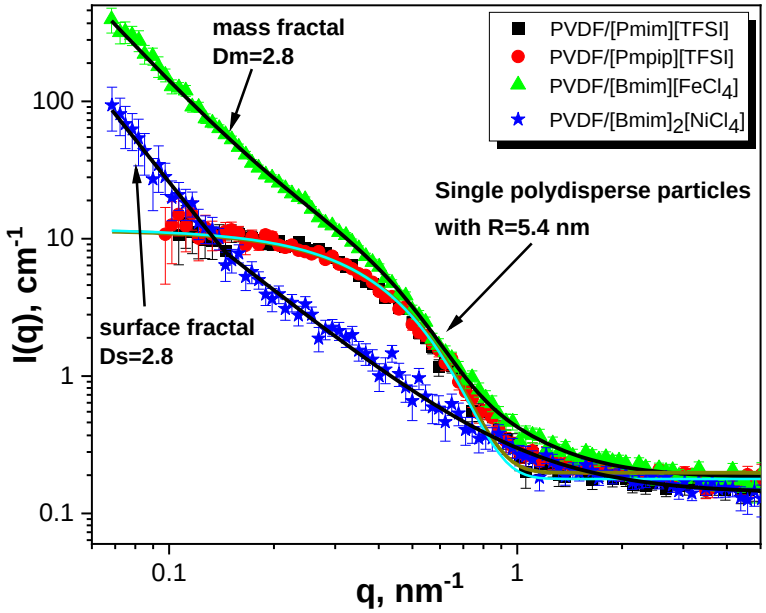

Figure 3. SANS data for polymer-IL based nanocomposties: PVDF/[Pmim][TFSI], PVDF/[Pmpip][TFSI], PVDF/[Bmim][$FeCl_4$] and PVDF/[Bmim]$_2$[$NiCl_4$]. Solid lines are fits according to various structural models.

The analysis of the SANS data presented in **Figure 3** allow to conclude that only single polydisperse "particles" (strictly speaking nanoinhomogeneities in the polymer matrix) are detected for composites PVDF/[Pmim][TFSI] and PVDF/[Pmpip][TFSI]. The radius of gyration of such particles, Rg=4.2nm, are the same for both samples and in case of spherical shape it can be estimated the average radius of such polydisperse spheres as R=5.4 nm. Thus, some nanoinhomogeneities are identified in the polymer matrix with characteristic size about 5 nm.

At the same time, single highly polydisperse nanoparticles with gyration radius Rg=4.9nm and large fractal-type aggregates (mass fractal dimension Dm=2.74) were observed by SANS for PVDF/[Bmim][$FeCl_4$]. The average radius of single particles for this composite, R=6.3nm, is larger than the one obtained for PVDF/[Pmim][TFSI] and PVDF/[Pmpip][TFSI] composites (there we have R=5.4nm). More complex and multiscale structures were observed for PVDF/$[Bmim]_2[NiCl_4]$ composite. Transition from mass fractal (power law exponent P=2.8 which corresponds to mass fractal dimension Dm=P=2.8) to surface fractal (power law exponent P=3.2 which corresponds to surface fractal dimension Ds=6-P=2.8) is observed for PVDF/$[Bmim]_2[NiCl_4]$ composites, correspondingly. Complex structural organization of structural units at lower size scale is also observed for such samples. The structural organization of the IL within the PVDF polymer matrix is summarized in **Figure 4**.

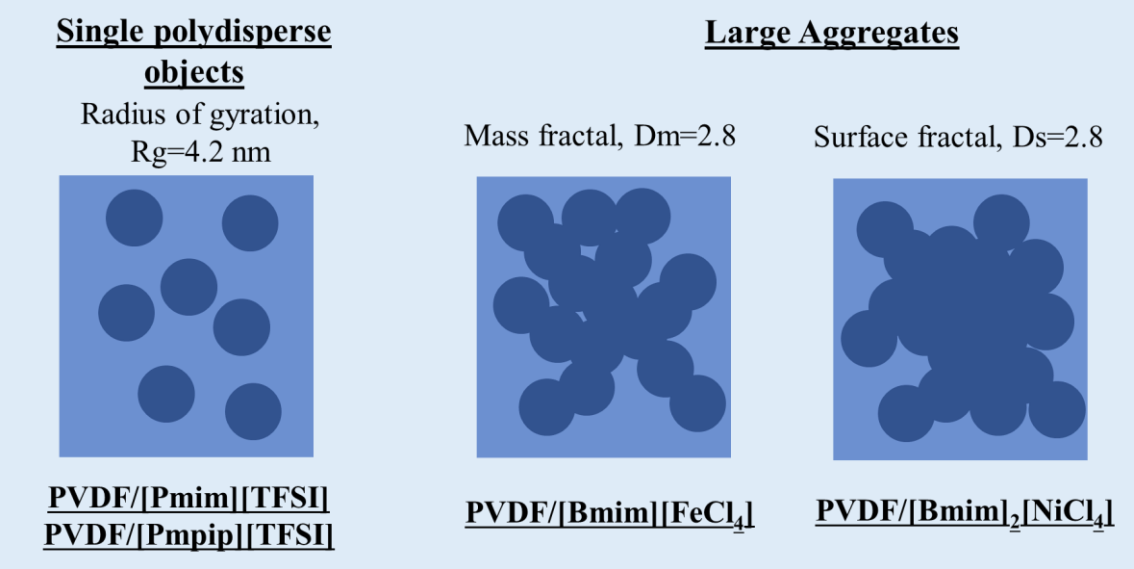

Figure 4. Sketches of the different structural organizations of the IL in: PVDF/[Pmim][TFSI], PVDF/[Pmpip][TFSI], PVDF/[Bmim][$FeCl_4$], and PVDF/$[Bmim]_2[NiCl_4]$.

Thus, the SANS results are in good agreement with the SEM images and macroscales. As observed from SEM images, the composites PVDF/[Pmim][TFSI] and PVDF/[Pmpip][TFSI] do not present a porous structure upon their processing into films. This fact is corroborated from SANS results in which only a single polydisperse objects are observed. The same behavior trend is not observed for the other IL-polymer based composites. Independently of the IL type both [Bmim][$FeCl_4$] and [Bmim]$_2$[$NiCl_4$] induce a porous structure, attributed to their structural organization with large aggregates. These results allow to infer that the interaction between these types of ILs with the DMF solvent during the evaporation process is higher when compared with the interaction with the [Pmim][TFSI] and [Pmpip][TFSI], resulting the presence of a porous structure. Thus, different structure organization at nanoscale which affect macroscopic properties of the composites are evidenced in the IL-polymer based films. These results corroborate the reported possible explanations concerning the porous morphology, the influence of ILs into the β phase content as a result of the strong interactions that occurs during the films processing between the polymer chains, the DMF solvent and the ILs. For this specific fluorinated matrix, the ion-dipole interactions occur through the interaction of the IL cation with the negative CF_2 groups present in PVDF matrix and also from the IL anion interactions with the PVDF holding CH_2 groups holding a positive charge [4, 10]. As briefly discussed, [Pmim][TFSI]/PVDF and [Pmpip][TFSI]/PVDF composites presented the high β contents, indicating that a single dispersion of the IL into the PVDF matrix favors the strong ion-dipole interactions (since the smaller particles size the larger specific surface to interact with environmental medium) between the PVDF chain and the IL charges, and in this sense the crystallinity of the developed materials.

Thus, the present work allows a fundamental understanding of IL-polymer systems, namely the IL-polymer interactions and the structuring of the IL within the polymer matrix, which in turn influences the different material properties such as morphological, physico-chemical, thermal, mechanical, and electrical. It is to notice that, in the last years, the main efforts in this field have been devoted to develop IL-polymer based functional materials with tailored responses based on IL intrinsic characteristics and on on the interaction between the polymer matrix and ILs. Based on this strategy, highly efficient materials have been developed for a new generation of applications such as piezo-ionic, and thermochromic, as well as for ionic- conductive materials, among others.

Further, polymer based nanocomposites and, in particular, the ones with the incorporation of ILs also present strong potential for novel application areas. As an example, by tuning the proper IL type and content, the reported variations at the nanostructure and morphology levels can find applications in the area of ferroelectret materials and devices for energy harvesting applications, since pore structure are essential in determining the final electrical properties and in the energy harvesting processes [43-45].

Thus, attending to the future perspectives in the area of IL-polymer based materials, this work emerges as a necessary step in the development of advanced IL-polymer based materials with tailored properties.

4. Conclusions

The present work reports on the effect of IL type in the structural, physical-chemical and ILs structural organization into the polymer matrix to a better understanding of the IL-polymer matrix chain interactions, stability and macroscopic response. For this purpose, different composites comprising different ILs were prepared.

The morphology depends both on IL type and IL/polymer/solvent interactions during the solvent evaporation process, displaying the samples comprising the magnetic ILs $[Bmim]_2[NiCl_4]$ and $[Bmim][FeCl_4]$ a porous structure. For IL-PVDF composites, an increase in the electroactive phase content occurs, being independent of the IL type. Additionally, no significant changes were observed in the thermal transitions of the composites, but a decrease in the melting temperature and thermal stability of PVDF matrix occurs upon the different ILs incorporation.

Different structural organization at nanoscale was observed by SANS for studied nanocomposites. Namely, just single polydisperse objects with Rg=4.2 nm was detected after addition of [Pmim][TFSI] or [Pmpip][TFSI] to PVDF and more complex structures were obtained for the composites PVDF/$[Bmim][FeCl_4]$ and PVDF/$[Bmim]_2[NiCl_4]$. Transition from just single polydisperse particles to mass fractal like or to surface like aggregation were concluded when [Pmim][TFSI] or [Pmpip][TFSI] was substituted by $[Bmim]_2[NiCl_4]$ or $[Bmim][FeCl_4]$ during synthesis process. Complex aggregation of particles observed in both $[Bmim]_2[NiCl_4]$/PVDF and $[Bmim][FeCl_4]$/PVDF composites indicate a strong interaction between these types of ILs with the DMF solvent during the evaporation process, resulting in the presence of a porous structure. In contrast, [Pmim][TFSI] and [Pmpip][TFSI] promotes strong interactions with PVDF polymer

chain as revealed by the higher β phase contents observed for this composite when compared to the composites incorporating $[Bmim]_2[NiCl_4]$ and $[Bmim][FeCl_4]$.

Acknowledgements

We thank the Fundação para a Ciência e Tecnologia- FCT, for financial support under the framework of the Strategic Funding UID/FIS/04650/2021, UIDB/50006/2020, UIDP/50006/2020, and LA/P/0008/2020, projects PTDC/FIS-MAC/28157/2017, and PTDC/BTM-MAT/28237/2017 and grants SFRH/BD/145345/2019 (LCF), and SFRH/BPD/121526/2016 (DMC). The authors thank funding by the Spanish State Research Agency (AEI) and the European Regional Development Fund (ERFD) through the project PID2019-106099RB-C43/AEI/ 10.13039/501100011033. and from the Basque Government Industry Department under the ELKARTEK program.

References

1. Oliveira, J., et al., *Polymer-based smart materials by printing technologies: Improving application and integration.* Additive Manufacturing, 2018. **21**: p. 269-283.
2. Aguilar, M.R. and J.S. Román, *Smart Polymers and Their Applications*. 2019: Elsevier Science.
3. Falahati, M., et al., *Smart polymers and nanocomposites for 3D and 4D printing.* Materials Today, 2020. **40**: p. 215-245.
4. Correia, D.M., et al., *Ionic Liquid–Polymer Composites: A New Platform for Multifunctional Applications.* Advanced Functional Materials, 2020. **30**(24): p. 1909736.
5. Zhang, S., et al., *Beyond solvents and electrolytes: Ionic liquids-based advanced functional materials.* Progress in Materials Science, 2016. **77**: p. 80-124.
6. Fernandes, L.C., et al., *Design of Ionic-Liquid-Based Hybrid Polymer Materials with a Magnetoactive and Electroactive Multifunctional Response.* ACS Applied Materials & Interfaces, 2020. **12**(37): p. 42089-42098.
7. Zhao, X., et al., *Hydrophobic ionic liquid-in-polymer composites for ultrafast, linear response and highly sensitive humidity sensing.* Nano Research, 2021. **14**(4): p. 1202-1209.
8. Correia, D.M., et al., *Cellulose Nanocrystal and Water-Soluble Cellulose Derivative Based Electromechanical Bending Actuators.* Materials, 2020. **13**(10).
9. Fernandes, L.C., et al., *Highly Sensitive Humidity Sensor Based on Ionic Liquid–Polymer Composites.* ACS Applied Polymer Materials, 2019. **1**(10): p. 2723-2730.
10. Correia, D.M., et al., *All printed soft actuators based on ionic liquid/polymer hybrid materials.* Applied Materials Today, 2021. **22**: p. 100928.
11. Meira, R.M., et al., *Ionic-Liquid-Based Electroactive Polymer Composites for Muscle Tissue Engineering.* ACS Applied Polymer Materials, 2019. **1**(10): p. 2649-2658.
12. Noshadi, I., et al., *Engineering Biodegradable and Biocompatible Bio-ionic Liquid Conjugated Hydrogels with Tunable Conductivity and Mechanical Properties.* Scientific Reports, 2017. **7**(1): p. 4345.
13. Bai, J., et al., *A novel ionic liquid polymer electrolyte for quasi-solid state lithium air batteries.* RSC Advances, 2017. **7**(49): p. 30603-30609.
14. Osada, I., et al., *Ionic-Liquid-Based Polymer Electrolytes for Battery Applications.* Angewandte Chemie International Edition, 2016. **55**(2): p. 500-513.
15. Correia, D.M., et al., *Magnetic ionic liquid/polymer composites: Tailoring physico-chemical properties by ionic liquid content and solvent evaporation temperature.* Composites Part B: Engineering, 2019. **178**: p. 107516.
16. Safarik, I., et al., *Cotton Textile/Iron Oxide Nanozyme Composites with Peroxidase-like Activity: Preparation, Characterization, and Application.* ACS Applied Materials & Interfaces, 2021. **13**(20): p. 23627-23637.
17. Yang, M., et al., *Dimethyl sulfoxide assisted dissolution of cellulose in 1-ethyl-3-methylimidazoium acetate: small angle neutron scattering and rheological studies.* Cellulose, 2019. **26**(4): p. 2243-2253.
18. Fedosse Zornio, C., et al., *Ionic PMMA/nanosilica interfaces from grafting ionic liquids under supercritical CO2 conditions.* European Polymer Journal, 2018. **109**: p. 82-92.

19. Stefanovic, R., et al., *Effect of halides on the solvation of poly(ethylene oxide) in the ionic liquid propylammonium nitrate.* Journal of Colloid and Interface Science, 2019. **534**: p. 649-654.
20. Brunner, M., et al., *Conformation of poly(ethylene glycol) in aqueous cholinium amino acid hybrid solvents.* Journal of Colloid and Interface Science, 2021. **602**: p. 334-343.
21. Hashimoto, K., et al., *Ion Gel Network Formation in an Ionic Liquid Studied by Time-Resolved Small-Angle Neutron Scattering.* The Journal of Physical Chemistry B, 2018. **122**(40): p. 9419-9424.
22. Apostolides, D.E., et al., *Near-Model Amphiphilic Polymer Conetworks Based on Four-Arm Stars of Poly(vinylidene fluoride) and Poly(ethylene glycol): Synthesis and Characterization.* Macromolecules, 2018. **51**(7): p. 2476-2488.
23. Kharel, A. and T.P. Lodge, *Coil Dimensions of Poly(ethylene oxide) in an Ionic Liquid by Small-Angle Neutron Scattering.* Macromolecules, 2017. **50**(21): p. 8739-8744.
24. Asai, H., et al., *Structural Analysis of High Performance Ion-Gel Comprising Tetra-PEG Network.* Macromolecules, 2012. **45**(9): p. 3902-3909.
25. Lee, H.-N., et al., *Unusual Lower Critical Solution Temperature Phase Behavior of Poly(ethylene oxide) in Ionic Liquids.* Macromolecules, 2012. **45**(8): p. 3627-3633.
26. Zhong, C., et al., *Syntheses, structures, and properties of a series of metal ion-containing dialkylimidazolium ionic liquids.* Bulletin of the Chemical Society of Japan, 2007. **80**(12): p. 2365-2374.
27. Meredith, M.B., et al., *Ambient temperature imidazolium-based ionic liquids with tetrachloronickelate(II) anions.* Polyhedron, 2009. **28**(12): p. 2355-2358.
28. Ribeiro, C., et al., *Electroactive poly(vinylidene fluoride)-based structures for advanced applications.* Nature Protocols, 2018. **13**(4): p. 681-704.
29. Kuklin, A.I., et al., *High-throughput SANS experiment on two-detector system of YuMO spectrometer.* Journal of Physics: Conference Series, 2018. **994**: p. 012016.
30. Soloviev, A.G., et al., *SAS program for two-detector system: seamless curve from both detectors.* Journal of Physics: Conference Series, 2017. **848**: p. 012020.
31. Mandal, D., K.J. Kim, and J.S. Lee, *Simple Synthesis of Palladium Nanoparticles, β-Phase Formation, and the Control of Chain and Dipole Orientations in Palladium-Doped Poly(vinylidene fluoride) Thin Films.* Langmuir, 2012. **28**(28): p. 10310-10317.
32. Fernandes, L.C., et al., *Ionic-Liquid-Based Printable Materials for Thermochromic and Thermoresistive Applications.* ACS Applied Materials & Interfaces, 2019. **11**(22): p. 20316-20324.
33. Silva, M.P., et al., *α- and γ-PVDF: Crystallization kinetics, microstructural variations and thermal behaviour.* Materials Chemistry and Physics, 2010. **122**(1): p. 87-92.
34. Mejri, R., et al., *Effect of anion type in the performance of ionic liquid/poly(vinylidene fluoride) electromechanical actuators.* Journal of Non-Crystalline Solids, 2016. **453**: p. 8-15.
35. Ferreira, J.C.C., et al., *Variation of the physicochemical and morphological characteristics of solvent casted poly(vinylidene fluoride) along its binary phase diagram with dimethylformamide.* Journal of Non-Crystalline Solids, 2015. **412**: p. 16-23.

36. Herstedt, M., et al., *Spectroscopic characterization of the conformational states of the bis(trifluoromethanesulfonyl)imide anion (TFSI−).* Journal of Raman Spectroscopy, 2005. **36**(8): p. 762-770.
37. Yassin, F.A., et al., *Highly effective ionic liquids for biodiesel production from waste vegetable oils.* Egyptian Journal of Petroleum, 2015. **24**(1): p. 103-111.
38. Correia, D.M., et al., *Ionic Liquid Cation Size-Dependent Electromechanical Response of Ionic Liquid/Poly(vinylidene fluoride)-Based Soft Actuators.* The Journal of Physical Chemistry C, 2019. **123**(20): p. 12744-12752.
39. Feigin, L. and D.I. Svergun, *Structure analysis by small-angle X-ray and neutron scattering*. Vol. 1. 1987: Springer.
40. Tomchuk, O.V., M.V. Avdeev, and L.A. Bulavin, *Modeling fractal aggregates of polydisperse particles with tunable dimension.* Colloids and Surfaces A: Physicochemical and Engineering Aspects, 2020. **605**: p. 125331.
41. Tomchuk, O.J.U.J.o.P., *The Concept of Fractals in the Structural Analysis of Nanosystems: A Retrospective Look and Prospects.* 2020. **65**(8): p. 709-709.
42. Schmidt, P.W.J.J.o.A.C., *Small-angle scattering studies of disordered, porous and fractal systems.* 1991. **24**(5): p. 414-435.
43. Zhang, Y., et al., *Ferroelectret materials and devices for energy harvesting applications.* Nano Energy, 2019. **57**: p. 118-140.
44. Mahanty, B., et al., *An effective flexible wireless energy harvester/sensor based on porous electret piezoelectric polymer.* Materials Chemistry and Physics, 2017. **186**: p. 327-332.
45. Ghosh, S.K., et al., *Self-poled Efficient Flexible "Ferroelectretic" Nanogenerator: A New Class of Piezoelectric Energy Harvester.* 2015. **3**(12): p. 1190-1197.